

Fluxoid fluctuations in mesoscopic superconducting rings

Julie A. Bert,¹ Nicholas C. Koshnick,¹ Hendrik Bluhm,^{1,*} and Kathryn A. Moler^{1,†}

¹*Departments of Physics and Applied Physics, Stanford University, Stanford, CA 94305*

(Dated: August 31, 2010)

Rings are a model system for studying phase coherence in one dimension. Superconducting rings have states with uniform phase windings that are integer multiples of 2π called fluxoid states. When the energy difference between these fluxoid states is of order the temperature so that phase slips are energetically accessible, several states contribute to the ring's magnetic response to a flux threading the ring in thermal equilibrium and cause a suppression or downturn in the ring's magnetic susceptibility as a function of temperature. We review the theoretical framework for superconducting fluctuations in rings including a model developed by Koshnick¹ which includes only fluctuations in the ring's phase winding number called fluxoid fluctuations and a complete model by von Oppen and Riedel² that includes all thermal fluctuations in the Ginzburg-Landau framework. We show that for sufficiently narrow and dirty rings the two models predict a similar susceptibility response with a slightly shifted T_c indicating that fluxoid fluctuations are dominant. Finally we present magnetic susceptibility data for rings with different physical parameters which demonstrate the applicability of our models. The susceptibility data spans a region in temperature where the ring transitions from a hysteretic to a non hysteretic response to a periodic applied magnetic field. The magnetic susceptibility data, taken where transitions between fluxoid states are slow compared to the measurement time scale and the ring response was hysteretic, decreases linearly with increasing temperature resembling a mean field response with no fluctuations. At higher temperatures where fluctuations begin to play a larger role a crossover occurs and the non-hysteretic data shows a fluxoid fluctuation induced suppression of diamagnetism below the mean field response that agrees well with the models.

PACS numbers: 73.23.Ra, 74.40.-n, 73.23.-b, 74.25.Ha, 74.25.Dw, 74.62.-c

I. INTRODUCTION

Fluctuations play an important role in the superconducting behavior of samples of reduced dimensionality:³ they can make electron pairing and long-range phase coherence occur at different temperatures in unconventional superconductors,⁴ lead to the Berezinskii-Kosterlitz-Thouless transition⁵ in two dimensions (2D), cause the destruction of long range phase order in infinitely long one-dimensional (1D) wires,⁶ and determine the resistive properties of 1D wires of finite length.⁷⁻¹⁰

We study the properties of superconducting 1D wires in a model system: uniform isolated aluminum rings. An applied magnetic field threading a mesoscopic superconducting ring drives transitions between states with different phase winding number (or number of fluxoids). The process of changing the fluxoid number by 2π is called a phase slip. Changes in fluxoid number also result in transitions between states with different angular momentum (or vorticity) with results in jumps in measurable quantities such as the current around the ring. The nature of superconducting fluctuations in rings has generated significant interest. Fluxoid dynamics in individual rings have been probed as a function of ring size,¹¹⁻¹³ magnetic field,^{12,14,15} and temperature.^{13,16,17} The occupation of metastable fluxoid states has also been measured to determine a crossover from 1D to 2D behavior in wide rings.^{18,19} Phase slip rates have been studied in both conventional low T_c [20] and unconventional high T_c [21] su-

perconducting rings. Ring inhomogeneities, such as weak links or nonuniform widths, have been studied as phase slip sites that can impact the ring's current-phase relationship and fluxoid transitions.^{15,22-26}

Transport measurements have long been used as a probe of superconducting fluctuations.^{27,28} These experiments measure a voltage that is directly related to the rate at which phase slips occur. In contrast, magnetic measurements such as ours are sensitive to the thermodynamic equilibrium current in the ring. Rather than tracking individual fluctuation events, this paper focuses on the effects of superconducting fluctuations on the ring's equilibrium supercurrent, I , as a function of applied flux, Φ_a , measured in a temperature range near the critical temperature, T_c . In order to reach equilibrium, phase slips must occur much faster than the measurement time. We focus on a regime, determined by the ring's physical parameters, where the distribution and switching between fluxoid states dominate the ring's equilibrium response to an applied field. Fluxoid states are the metastable superconducting solutions which correspond to local minima of the Ginzburg-Landau free energy functional and can be labeled by an integer phase winding number. In thermal equilibrium, when the ring's limited thermal energy is sufficient to cross the barrier between fluxoid states but still small compared to the saddle point energy, it spends almost no time near the saddle point solutions that allow phase slips. As a result, our equilibrium measurement of the ring current depends only on

the energy difference between fluxoid states.

Theoretical work using Ginzburg-Landau (GL) theory has predicted the current in the presence of an applied flux threading the ring in the opposite limit, where fluctuations between states with different fluxoid numbers are inadequate to describe the response in the presence of all possible fluctuations including local phase and amplitude fluctuations. Ambegaokar and Eckern applied a Gaussian approximation to GL to predict a mesoscopic persistent current driven by superconducting fluctuations above T_c ,^{29,30} which decreased exponentially with increasing T on the scale of the correlation energy. However, the Gaussian approximation, accurate far above T_c where the quadratic term in the GL free energy dominates, diverges as T approaches T_c . von Oppen and Riedel used a transfer matrix approach to GL theory that accounts for all thermal fluctuations above and below T_c to calculate the supercurrent and correct the divergence at T_c .² Schwiete and Oreg then proposed a simplification of the full von Oppen and Riedel (VOR) theory that makes an analytic prediction for the ring's susceptibility, $dI/d\Phi_a$, in the limit where the superconducting coherence length is on the order of the radius,³¹ which provides a simple alternative to solving the VOR model numerically.

Direct measurements of the ring current as a function of applied flux are useful because it provides access to the thermodynamic free energy through the derivative $I = -\partial F/\partial\Phi_a$. While there are also interesting features in the full flux dependence,³² the fluctuation response is well captured by the zero field susceptibility. Consequently, in this paper we measure the ring's zero field susceptibility as a function of temperature, $dI(T)/d\phi|_{\phi=0}$, where $\phi \equiv \Phi_a/\Phi_0$ and $\Phi_0 \equiv h/2e$ is the superconducting flux quantum.

A number of different experiments have used susceptibility measurements to study fluctuations in individual superconducting rings.^{13,20,23,32,33} Zhang and Price studied the phase slip rate and susceptibility as a function of temperature in a single Al ring.²⁰ The ring's geometry and long mean free path favored amplitude fluctuations that were expected to support a susceptibility response above T_c . However, the observed susceptibility signal was an order of magnitude larger than predicted by GL theory. Koshnick *et al.*³² measured the susceptibility of 15 individual rings with long mean free paths as a function of Φ_a . All rings showed a fluctuation induced susceptibility response above T_c . The magnitude of the fluctuation signal was large in the Little-Parks region, where an applied flux suppresses the ring's $T_c(\Phi_a)$ below its zero field value, $T_c(\Phi_a = 0)$. The susceptibility responses of all the rings in that measurement were well described by von Oppen and Riedel's complete GL model.²

Dirtier rings or rings with narrower geometries should exhibit fluxoid fluctuations. Instead of generating an enhancement in the susceptibility above T_c , fluxoid fluctuations can suppress the superconducting response well below T_c . This paper focuses on rings that are likely to

experience fluxoid fluctuations. We start by describing the different thermal fluctuations, namely phase slips and fluxoid fluctuations, experienced by our rings in Sec. II A. We then establish the physical conditions that support fluxoid fluctuations in Sec. II B. We outline a theory¹ where a thermal distribution of fluxoid states suppresses the rings diamagnetism (Sec. II C). Our theoretical analysis concludes by comparing our fluxoid only model to a complete theory that includes all thermal fluctuations in the GL framework² (Sec. II D), where we find good agreement in rings where fluxoid fluctuations dominate the response. We finally discuss our measurement technique in Sec. III and present data from two sets of ring samples with different mean free paths, which we compare to the theoretical models (Sec. III C).

II. FLUCTUATION THEORY

We begin by describing the different types of thermal fluctuations encountered in the GL formalism applied to a ring geometry, paying particular attention to the difference between phase slips (processes that change the fluxoid number by moving through a saddle point in configuration space) and fluxoid fluctuations (fluctuations in fluxoid number based on the energy difference between fluxoid states). We then discuss the onset of thermal equilibrium by considering the phase slip theory of Langer and Ambegaokar⁷ as formulated for rings^{20,34} in the context of our actual measurement. Finally, we introduce fluctuation models that illuminate how different types of fluctuations influence the ring's susceptibility response. These models include a mean field model with no fluctuations, a model that includes only fluxoid states, the VOR model including all thermal fluctuations in the GL framework, and a harmonic oscillator approximation of the VOR model that includes only quadratic fluctuations. By comparing these models we can determine the type of fluctuations that dominate the response at different temperatures and for rings with different physical parameters.

A. Types of Fluctuations

In the context of GL formalism we introduce a complex order parameter, $\psi(\mathbf{r})$, with an associated amplitude and phase. Fluctuations in the amplitude and phase of the order parameter are deviations in ψ from the mean field solutions corresponding to local minima of the GL free energy. Fluctuations play a large role when the thermal energy of the system allows multiple wavefunctions to contribute to the ring's properties.

The ring geometry of our samples imposes a constraint on the order parameter phase. The periodic boundary condition requires that the phase be single valued, meaning it must wind by an integer multiple of 2π around the ring. A phase slip is the process of changing

the phase winding number by 2π . They usually occur by briefly suppressing superconductivity in a coherence-length-sized section of the ring.³ Rings whose circumference, L , is longer than the superconducting coherence length, $\xi(T)$, have multiple metastable states that differ by a phase winding or fluxoid number and their homogeneous superfluid density. In a temperature range where phase slips occur within the measurement time, the ring fluctuates between its minimum energy fluxoid state and the metastable fluxoid states.³⁵ Such occupation of multiple fluxoid states or fluxoid fluctuations can contribute to a suppression of the ring's superconducting response.

B. Phase Slips and Equilibrium

The ring's measured response represents its thermal equilibrium response when phase slips occur at a rate that is fast compared to experimental time scales (~ 10 ms), and no hysteresis is observable. In this section we derive a condition for the onset of phase slips and a separate condition for the onset of fluxoid fluctuations.

We study switching between states driven by phase slips by adapting the theory of Langer and Ambegaokar.⁷ Langer and Ambegaokar's treatment assumes a 1D superconductor where the cross-section is smaller than the superconductor's coherence length, $\xi(T)$, and penetration depth, $\lambda(T)$, so ψ has no radial variation. This assumption is particularly useful since exact solutions that minimize the GL free energy exist for 1D systems. Additionally Langer and Ambegaokar consider a homogeneous superconductor making phase-slips equally likely at any point along the ring's circumference. Langer and Ambegaokar's theory with a correction to the prefactor by McCumber and Halperin⁸ predicts a phase slip rate by calculating the lowest energy pathway between two fluxoid states as defined by the energy barrier for the saddle point in wave function configuration space. Each fluxoid state, with energy F_{\min} and phase winding $2\pi n$, represents a stable local minima of the GL free energy functional. The saddle point energies, F_{saddle} , being stationary points of the free energy, must also satisfy the GL equations; however, these solutions represent unstable configurations. The phase slip rate, Γ , then depends exponentially on the energy barrier $\Delta F(T, \phi) = F_{\text{saddle}}(T, \phi) - F_{\min}(T, \phi)$.

$$\Gamma = \Omega \exp\left(-\frac{\Delta F(T, \phi)}{k_B T}\right) \quad (1)$$

The prefactor, $\Omega = (L/\xi)(\Delta F/k_B T)^{1/2}/\tau$, was corrected by McCumber and Halperin based on arguments using the time dependent Ginzburg Landau model,⁸ where $\tau = \pi\hbar/8k_B(T_c - T)$ is the relaxation time. For phase slips to occur at a rate of 100 Hz, a rate that is approximately equal to our measurement time, the energy difference $\Delta F/k_B T$ may not exceed ~ 20 . Although the prefactor is large, $\Omega \approx 5 \times 10^{11} - 5 \times 10^{12}$ Hz, the exponential dependence overwhelms changes in the prefactor

which can therefore be ignored. We find an approximate condition for the onset of phase slips from calculations of the energy barrier ΔF .

We find expressions for F_{\min} and F_{saddle} which represent stationary points of the GL free energy. One dimensional Ginzburg-Landau theory introduces the GL free energy functional in the presence of a magnetic field represented by the vector potential \vec{A} as

$$F[\psi(x)] = \int \left[\alpha |\psi(x)|^2 + \frac{1}{2} \beta |\psi(x)|^4 + \frac{\hbar}{2m^*} \left| \left(\vec{\nabla} - \frac{ie^* \vec{A}}{\hbar} \right) \psi(x) \right|^2 \right] d^3x. \quad (2)$$

α and β both depend on T , and $\alpha^2/\beta = B_c(T)^2/\mu_0$ is related to the superconducting critical field, $B_c(T)$. e^* and m^* are the charge and mass of the Cooper pairs and μ_0 is the permeability of free space.

We look for stable solutions that locally minimize the Ginzburg Landau free energy functional. In a homogeneous one dimensional ring fluxoid states have free energies

$$F_{\min}(T, \phi) = -F_c(T) \left(1 - \frac{\xi(T)^2}{R^2} (\phi - n)^2 \right)^2, \quad (3)$$

where the critical field, and the ring volume ($V = 2\pi Rwd$) determine the ring's total condensation energy ($F_c(T) = VB_c(T)^2/2\mu_0$). w is the ring width and d is the thickness. The dependence on $\xi(T)/R$ accounts for the suppression of the superfluid density by the phase gradient around the ring with coherence length $\xi(T)$ and radius R . The Aharonov-Bohm flux, $\phi = \Phi_a/\Phi_0$, can be transformed into a shift in the boundary conditions for a wave function in a ring,³⁶ and therefore contributes to the energy in the same way as n .

To find the saddle point energies, Zhang applied Langer and Ambegaokar's phase slip theory to a ring geometry,³⁴ and by used the approximation $L \gg \xi(T)$ to calculate the saddle point energy

$$F_{\text{saddle}}(T, \phi) = F_c(T) \left(\frac{8\sqrt{2\delta(T, \phi, n)} \xi(T)}{3L} - \frac{(2 + \delta(T, \phi, n))^2}{9} \right) \quad (4)$$

where $L = 2\pi R$ is the ring's circumference and $\delta(T, \phi, n)$ is the normalized difference between the square of the order parameter amplitudes near and far from a phase slip event. $\delta(T, \phi, n)$ is a real number between 0 and 1 that satisfies the relation

$$2\pi n = \sqrt{\frac{1-\delta}{3}} \frac{L}{\xi(T)} + 2 \tan^{-1} \left(\sqrt{\frac{3\delta}{2(1-\delta)}} \right) + 2\pi\phi. \quad (5)$$

For $\phi = n + 1/2$, $\delta = 1$.

We are interested in a regime where $L \gg \xi(T)$, and δ remains close to one for moderate n . Using the substitution $\kappa = \sqrt{1 - \delta}$ and expanding to lowest order in κ , we arrive at a simplified expression for δ .

$$\delta(T, \phi, n) = 1 - \left(\frac{\sqrt{3}\pi(2n - 2\phi - 1)}{\frac{L}{\xi(T)} - 2\sqrt{2}} \right)^2 \quad (6)$$

Returning to the energy expression, Eq. (4), we find minima of F_{saddle} at $n - \phi = 1/2$

$$\min(F_{\text{saddle}}) = F_c(T) \left(\frac{8\sqrt{2}\xi(T)}{3L} - 1 \right). \quad (7)$$

The energy expressions for F_{min} (Eq. (3)) and F_{saddle} (Eq. (4)) are plotted as a function of flux for different fluxoid number n in Fig. 1. The minimum value of F_{saddle} given in Eq. (7) is also plotted. The plots demonstrate how an increase in the ratio $L/\xi(T)$ decreases the variation of both F_{min} and F_{saddle} with applied flux. For $L/\xi(T) = 30$ the variation in $\Delta F(\phi)$ between $\phi = 0$ and $\phi = 1/2$ is 30% of $\Delta F(\phi = 0)$. This variation decreases to 12% for $L/\xi(T) = 80$.

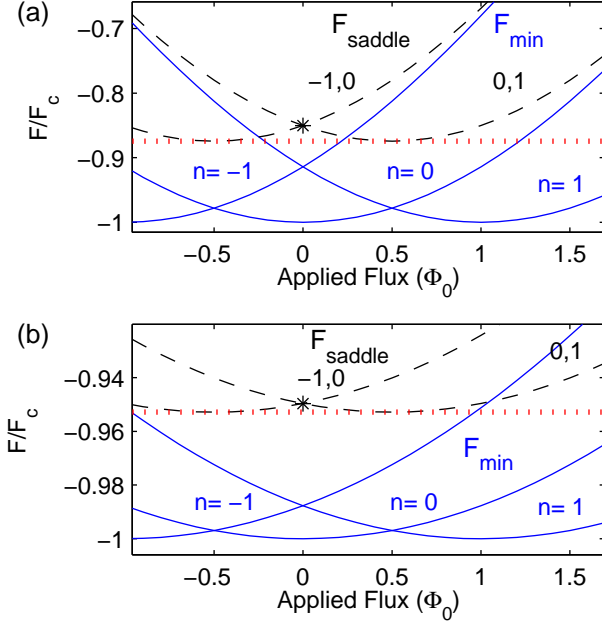


FIG. 1: (Color Online) Free energy of fluxoid states (blue solid line, Eq. 3) and saddle point energies (black dashed line, Eq. 4) as a function of applied flux, in units of the condensation energy, F_c . The red dotted line is the minimum value of F_{saddle} which is approximately equal to 3.8 times the condensation energy for a ring section of length ξ . (a) The respective energies when $L/\xi(T) = 30$. (b) The respective energies when $L/\xi(T) = 80$. The energy barrier between adjacent fluxoid states, $\Delta F_{\text{min}}^{\pm 1,0} = F_{\text{min}}^{n=\pm 1} - F_{\text{min}}^{n=0}$, scales differently than the saddle point energy ΔF .

As $L/\xi(T)$ becomes increasingly large, in rings with long circumferences, the flux dependence of both $F_{\text{saddle}}(T, \phi)$ and $F_{\text{min}}(T, \phi)$ becomes less important to the energy barrier $\Delta F(T, \phi)$. This decreasing dependence on flux justifies the approximation that neither F_{min} nor F_{saddle} depends on the flux in rings where $L \gg \xi(T)$. Approximating $F_{\text{saddle}}(T, \phi) \approx \min(F_{\text{saddle}})$ and $F_{\text{min}}(T, \phi) \approx \min(F_{\text{min}})$, leaves $\Delta F(T) \approx 3.8wd\xi B_c(T)^2/2\mu_0$, which is also independent of flux. The exponential dependence of the phase slip rate combined with the large attempt frequency Ω in Eq. (1) imply phase slips occur when $\Delta F(T) \lesssim 20k_B T$. Qualitatively this result makes sense because it states that phase slips occur when there is sufficient thermal energy to suppress the order parameter on the scale of the coherence length. This energy scale differs from the ring's total condensation energy, F_c , which is proportional to the volume of the entire ring.

In contrast to the phase slip energy we just derived, the we obtain the energy associated with each fluxoid state by expanding the mean field GL free energy expression, Eq. (3), to lowest order in $\xi(T)/R$.

$$F_{\text{min}}^n(T, \phi) = \frac{I^0(T)\Phi_0}{2}(\phi - n)^2 - V \frac{B_c(T)^2}{\mu_0} \quad (8)$$

where

$$I^0(T) = \frac{2VB_c(T)^2\xi(T)^2}{\Phi_0\mu_0R^2} = \frac{4\pi^2k_B T L^2}{\Phi_0\xi(T)^2\gamma(T)} \quad (9)$$

We introduce the parameter $\gamma(T)$ which describes the inverse phase stiffness of the ring. Rings with a larger $\gamma(T)$ are more likely to exhibit fluxoid fluctuations. $\gamma(T)$ is discussed in more detail in section II D.

When the energy difference between the lowest energy fluxoid states, $\Delta F_{\text{min}}^{\pm 1,0} = F_{\text{min}}^{n=\pm 1} - F_{\text{min}}^{n=0}$, is comparable to the temperature, multiple fluxoid states contribute to the ring's equilibrium response.

The criterion for phase slips ($\Delta F(T) \approx 3.8wd\xi B_c(T)^2/2\mu_0$) scales differently with ring radius compared to the energy difference between fluxoid states ($\Delta F_{\text{min}}^{\pm 1,0}(T) \approx 4\pi wd\xi B_c(T)^2/2\mu_0(\xi/R)$) that determines onset temperature for fluxoid fluctuations. As stated above phase slips begin when $\Delta F(T) \lesssim 20k_B T$, while fluxoid fluctuations onset for $\Delta F_{\text{min}}^{\pm 1,0} \lesssim 6k_B T$. See section II C Eq. (13). These two types of fluctuations onset at the same temperature when $\xi(T)/L = 0.014$. Therefore, in the limit where $L \gg \xi(T)$ (specifically when $\xi(T)/L < 0.014$), the condition for fluxoid fluctuations is already satisfied when phase slips begin to occur. By applying the fluxoid condition, Eq. (13), and making an approximation that $T \approx T_c$ we can remove the temperature dependence and rewrite the condition as $\gamma(T_c) > 16,000$. As a result, in the longest wires with the largest $\gamma(T)$ a suppression of the response due to fluxoid fluctuations is expected as soon as the ring is able to reach thermal equilibrium.

In the opposite limit, for small clean rings, if the condition $\Delta F_{\text{min}}^{\pm 1,0} \lesssim 6k_B T$ is not met by the time $\Delta F(T) \approx$

$k_B T$ then thermal occupation of the saddle point solutions and other higher energy states become significant. This occurs in rings where $\gamma(T_c) < 40$. When fluxoid fluctuations onset they will not dominate the fluctuation response and their effect on the zero-field susceptibility is negligible.

Using Eq. 1 we can predict the onset of phase slips in aluminum rings. A ring with a mean free path $\ell_e = 4$ nm has $\lambda(0) \approx 800$ nm and $\xi(0) \approx 85$ nm.³³ Using standard temperature dependencies for these parameters, $\xi(T) \propto (1-t)^{-1/2}$ and $\lambda(T) \propto (1-t)^{-1/2}$ where $t = T_c/T$,³⁷ a ring of this material with $w = 80$ nm and $d = 40$ nm will have switching occur on experimental time scales down to 1.1 K when $T_c \approx 1.24$ K, while a ring with $d = 1$ nm will continue to have phase slips down to 0.45 K.

We have shown that the onset temperature for phase slips, $\Delta F \propto \xi(T)$, and for fluxoid fluctuations, $\Delta F_{\min}^{\pm 1,0} \propto \xi(T)^2/R$, scale differently with the ring radius. However, the presence of phase slips is a precondition for fluxoid fluctuations. The phase slip rate, Eq. (1), depends on the temperature and the energy difference between the saddle point energy and the minimized GL energy. In the $L \gg \xi(T)$ limit, the rate is independent of applied flux and the ring circumference, $\Gamma \propto \exp(-3.8wd\xi(T)B_c(T)^2/2\mu_0k_B T)$. This phase slip rate and the measurement time sets our criterion for equilibrium. Namely a ring's measured response represents its equilibrium response when phase slips occur faster than the time over which the flux is swept through the transition region.

In the following sections we explore the effects of fluctuations on the ring's response in thermal equilibrium. Each of the models presented below includes a different set of fluctuations. By comparing the model predictions for different ring parameters we can pinpoint the effect of different fluctuations on ring response and set a physical regime where each of the fluctuations will dominate. Specifically we find that in rings with weak phase stiffness a model including only fluxoid fluctuations accurately reproduces the ring response except for an apparent shift in T_c indicating that fluxoid fluctuations dominate.

C. Fluxoid Number Distribution Model

We start with a model that includes only fluxoid fluctuations: fluctuations caused by integer winding or unwinding of the phase of the order parameter. This model is not complete because it does not include nonuniform phase fluctuations or amplitude fluctuations. Put another way this model includes only the large fluctuations between local minima in the GL free energy (see Fig. 1), and ignores all the small fluctuations about each local minimum as well as the saddle points and intermediate states. It is instructive to develop this model because comparisons between this fluxoid only model and more complete models shed light on what portion of the fluctuation response of a ring is due to solely to fluxoid fluctuations.

As discussed in the previous section, we expect this model to be valid for rings with $\gamma(T_c) > 40$.

We return to the mean field 1D GL free energy, Eq. (3), which is related to the ring current by $I = -\partial F/\partial \Phi_a$. Taking the derivative yields an expression for the ring current of a state with n fluxoids.

$$I_n(T, \phi) = I^0(T)(\phi - n) \left(1 - \frac{\xi(T)^2}{R^2}(\phi - n)^2 \right) \quad (10)$$

where $I^0(T)$ was given in Eq. (9). $I^0(T)(\phi - n)$ is the Meissner response which decreases linearly with increasing temperature close to T_c , while the cubic term arises from pair-breaking.

The energy associated with each fluxoid current state, F_{\min}^n , was derived in the previous section, Eq. (8). If phase slips occur at a high enough rate, so that the metastable fluxoid states are in thermal equilibrium as discussed in the previous section, we can model^{3,33} the resulting current response as a Boltzmann distribution of fluxoid states.

$$I_F(T, \phi) = \frac{\sum_n I_n(T, \phi) \exp(-F_{\min}^n(T, \phi)/k_B T)}{\sum_n \exp(-F_{\min}^n(T, \phi)/k_B T)}. \quad (11)$$

We call the total ring current generated by fluxoid states I_F to distinguish it from the total ring current including all fluctuation states that will be presented in the next section. The susceptibility response of the ring at zero applied flux, $dI(T)/d\phi|_{\phi=0}$ gives us access to the thermodynamic free energy. In our rings $\xi(T)/L \ll 1$, so we make the approximation $I_n(T, \phi) \approx I^0(T)(\phi - n)$. The derivative of the total ring current at $\phi = 0$ is

$$\left. \frac{dI_F(T)}{d\phi} \right|_{\phi=0} = I^0(T) \left(1 - \frac{\sum_n 2\sigma n^2 \exp(-\sigma n^2)}{\sum_n \exp(-\sigma n^2)} \right) \quad (12)$$

where $\sigma \equiv I^0(T)\Phi_0/2k_B T$. Eq. (12) shows that including a distribution of fluxoid states reduces the ring's susceptibility response from the mean field value, $I^0(T)$. However, the ring's superfluid density is not reduced. The second term in Eq. (12) is proportional to the RMS fluctuation of the fluxoid number, n . The magnitude of the reduction in susceptibility depends on σ . When σ is large, terms with $n \neq 0$ are small and the susceptibility is approximately equal to the mean field value. When σ is small, the $n = \pm 1$ terms begin to play a significant role. We define a criterion¹ for fluxoid fluctuations to reduce the Meissner response by more than 5% when

$$\frac{dI_F(T)}{d\phi} \approx I^0(T) < \frac{12k_B T}{\Phi_0}, \quad (13)$$

as long as phase slips occur at a sufficiently high rate. We used this criterion in section II B to compare the onset of fluxoid fluctuations and phase slips. In plots of the susceptibility vs. temperature we observed a suppression below the mean field value for susceptibilities below this cutoff. This downturn in the susceptibility signal, which occurs at T less than T_c , is a hallmark of

the suppression of the diamagnetic response by fluxoid fluctuations. More specifically, as stated in section II B we expect a visible downturn in rings with $\gamma(T_c)$ values between 40 and 16000. Rings with $\gamma(T_c) < 40$ will not show a downturn as higher energy fluctuations overwhelm fluxoid fluctuations. In rings with $\gamma(T_c) > 16,000$ fluxoid fluctuations will occur as soon as thermal equilibrium is reached. These rings will exhibit a response that is already suppressed below the mean field value for all data taken in thermal equilibrium. The next sections will be devoted to developing more complex models which include a more complete set of thermal fluctuations.

Thus far, we have considered a fluxoid model that predicts the existence of the downturn in susceptibility below T_c . In some rings, near $T = T_c$, the $R \gg \xi(T)$ assumption we made to obtain Eq. (8) and (12) is not strictly valid. As a result, the energy between successive metastable states can no longer be approximated by the expansion in Eq. (8). By including the quartic term of Eq. (3), the GL free energy vanishes rather than increasing indefinitely for $\phi - n > L/\xi(T)$. Thus, the Boltzmann distribution, Eq. (11), is also not well defined because summing over all n leads to a divergent denominator. The numerator on the other hand remains finite since states with $\phi - n > L/\xi(T)$ do not contribute. Furthermore, our treatment thus far has ignored phase fluctuations that are not uniform around the ring and all amplitude fluctuations.

D. von Oppen and Riedel Model

To address these issues, we compare our simple fluxoid model to the model of von Oppen and Riedel,² VOR, which generates numeric solutions that include all thermal fluctuations within the GL framework in homogeneous rings. Applying a harmonic oscillator approximation to the VOR model, discussed in the next section, provides a direct mathematical connection between the VOR and fluxoid model discussed in the previous section.

Following von Oppen and Riedel,² we begin with the expression for the GL energy functional given in Sec. II Eq. (2). We map the free energy onto a one dimensional ring geometry with no lateral variation of the order parameter so $\psi(r, z, \theta) = \psi(\theta)$ and $dx^3 = wdRd\theta$. We can then redefine $Rd\theta$ as dx .

We rewrite Eq. (2) using reduced variables $\psi(x) = \bar{\psi}(\bar{x})\sqrt{|\alpha|/\beta}$, $\bar{\nabla} = \xi\nabla$, and $x = \bar{x}\xi$. $\xi(T)$ is the superconducting coherence length and is given by $\xi(T) = \hbar/\sqrt{2m^*\alpha}$.

$$F[\bar{\psi}(\bar{x})] = E_0(T)k_B T \int_{-\Lambda(T)/2}^{\Lambda(T)/2} \left[\eta |\bar{\psi}(\bar{x})|^2 + \frac{1}{2} |\bar{\psi}(\bar{x})|^4 + \left| \left(\bar{\nabla} - \frac{2\pi i}{\Lambda(T)} \phi \right) \bar{\psi}(\bar{x}) \right|^2 \right] d\bar{x} \quad (14)$$

η is $+1(-1)$ for temperatures above (below) the superconducting critical temperature T_c . $\Lambda(T)$ is the reduced circumference $\Lambda(T) = L/\xi(T) = \sqrt{8\pi k_B |T - T_c|/E_c}$ and $E_0(T)k_B T = wd\xi(T)B_c(T)^2/\mu_0$ is the condensation energy of a ring section of length $\xi(T)$. The correlation energy for the ring, $E_c = \pi^2 \hbar v_f \ell_e / 3L^2$, includes the mean free path, ℓ_e , and the fermi velocity, v_f , which is 2.03×10^6 m/s in aluminum. $E_0(T)$ can also be written as

$$E_0(T) = \frac{(2\pi)^{5/2}}{21\zeta(3)} \left(\frac{k_B |T - T_c|}{E_c} \right)^{3/2} \frac{E_c M_{\text{eff}}}{k_B T}, \quad (15)$$

where $\zeta(3) = 1.021$ is the Riemann zeta function. $M = k_f^2 wd/4\pi$ is the number of transverse channels. k_f is the fermi wave vector, which for an aluminum ring is $k_f = 1.75 \times 10^{10} \text{ m}^{-1}$. Including disorder results in an effective number of channels, $M_{\text{eff}} = M\ell_e/L$.

We obtain the thermodynamic expression of the current from the flux derivative of the ring's partition function.

$$I(T, \phi) = -k_B T \frac{1}{Z_{sc}} \frac{\partial}{\partial \Phi_a} Z_{sc} \quad (16)$$

The partition function is the path integral of the GL energy.

$$Z_{sc} = \int [d\bar{\psi}(\bar{x})][d\bar{\psi}^*(\bar{x})] \exp \left(\frac{-F[\bar{\psi}(\bar{x})]}{k_B T} \right) \quad (17)$$

The VOR model uses a transfer matrix technique³⁸ to map the Ginzburg-Landau path integral partition function, Eq. (17), onto another partition function

$$Z = \sum_{l=-\infty}^{\infty} \exp(-i2\pi l \phi) \sum_{n=0}^{\infty} \exp(-2E_0(T)\Lambda(T)\mathcal{E}_{n,l}) \quad (18)$$

where $\mathcal{E}_{n,l}$ are the eigenvalues of the fictitious 2D single-particle Hamiltonian,

$$H = -\frac{1}{8E_0(T)^2} \nabla^2 + \frac{1}{2} \eta \vec{r}^2 + \frac{1}{4} \vec{r}^4. \quad (19)$$

We define $\vec{\rho} = (2E_0(T))^{1/3} \vec{r}$ and rewrite Eqs. (18) and (19) to emphasize the parameter $\gamma(T)$.³²

$$Z = \sum_{l=-\infty}^{\infty} \exp(-i2\pi l \phi) \sum_{n=0}^{\infty} \exp(-\gamma(T)^{1/3} \mathcal{E}_{n,l}) \quad (20)$$

$$H = -\frac{1}{2} \nabla^2 + \frac{1}{2} \frac{\Lambda(T)^2}{\gamma(T)^{2/3}} \vec{\rho}^2 + \frac{1}{4} \vec{\rho}^4 \quad (21)$$

The temperature dependence is set by the coherence length through the relation $\Lambda(T) = L/\xi(T)$. The parameter

$$\gamma(T) \equiv \frac{\Lambda(T)^3}{2E_0(T)} = \frac{42\zeta(3)}{\pi} \frac{k_B T}{M_{\text{eff}} E_c} \quad (22)$$

can be thought of as a measure of inverse phase stiffness, which determines the type of fluctuations that dominate the ring's susceptibility response.³² The definition of γ introduced in Koshnick *et al.*³² made the approximation $T \approx T_c$. The larger temperature range explored in this paper makes it necessary to reintroduce the T dependence. We use the relation for $I^0(T)$ given in the second part of Eq. (9) to compare the VOR model to the mean field and fluxoid models.

Eqs. (20) and (21) can be solved numerically. The Hamiltonian can be rewritten as a harmonic oscillator with a quartic perturbation. We can then write matrix elements in terms of the coefficients and diagonalized numerically to find the eigenvalues.^{34,39} The eigenvalues are used in the partition function, Eq. (20), and substituted into the thermodynamic equation for the current, Eq. (16), to generate the full current response. We find the zero-field susceptibility by taking a derivative with respect to applied flux at $\phi = 0$.

Analytic solutions can be instructive, and as a result it is useful to find approximations to the full VOR model that are valid over some set of ring parameters or temperatures. One such approximation is to ignore the quartic perturbation to the Hamiltonian, which then takes the form of a simple harmonic oscillator.

E. Harmonic Oscillator Model

The harmonic oscillator (HO) approximation is valid at temperatures well below T_c , where the wave functions contributing to Eq. (20) only extend over a narrow region around the minimum of the Mexican hat potential of Eq. (21), so that the latter can be approximated by a quadratic expansion. In this case, fluctuations from the quartic nature of the potential should not play a significant role. We refer to the fluctuations in this model as quadratic fluctuations, rather than Gaussian fluctuations, to avoid confusion with small order parameter fluctuations above T_c , which are often referred to as Gaussian fluctuations.

Eigenstates have the form $\vec{r} = |r| \exp(il\phi)$, so Eq. (21) can be written as a 1D problem, $H = -\frac{1}{2} \frac{d^2}{dr^2} + V(r)$ where

$$V(r) = \frac{l^2}{2r^2} + \frac{1}{2} \frac{\Lambda(T)^2}{\gamma(T)^{2/3}} r^2 + \frac{1}{4} r^4. \quad (23)$$

Expanding $V(r)$ about its minimum at $R_m(l)$ leads to the eigenvalues

$$\mathcal{E}_{n,l} = \frac{l^2}{2R_m(l)^2} + \frac{R_m(l)^4}{4} + \omega(n + 1/2) \quad (24)$$

where $\omega = \sqrt{\Lambda(T)^2/\gamma(T)^{2/3} + 3R_m(l)^2 + 3l^2/R_m(l)^4}$.

Only terms that change with l , the angular momentum coordinate in the fictitious Hamiltonian, contribute to the flux dependence of the partition function, thus

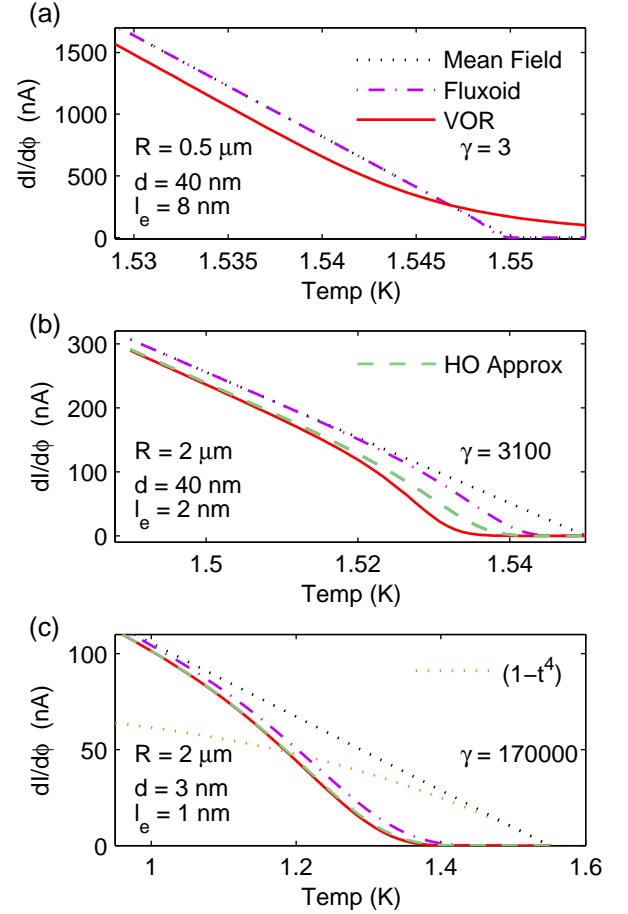


FIG. 2: (Color Online) Theoretical susceptibilities calculated using the mean field model, black dotted line Eq. (9), the fluxoid model, purple dot-dash line Eq. (12), the VOR model, red solid line Eqs. (16, 20, 21), and its approximate HO solution, green dashed line Eqs. (16, 26), for rings with $w = 80 \text{ nm}$ and $T_c = 1.55 \text{ K}$. a) $\gamma(T = T_c) = 3$. The VOR model predicts a susceptibility above T_c . b) $\gamma(T = T_c) = 3100$. A downturn occurs at $dI/d\phi \approx 12k_B T/\Phi_0 \approx 120 \text{ nA}$, $T \approx 1.52 \text{ K}$. The fluxoid, HO and VOR models reproduce the overall lineshape of the downturn, up to an offset in T_c . However, the three models predict downturns of different sizes with the largest predicted by the VOR model. c) $\gamma(T = T_c) = 170,000$ Fluxoid fluctuations dominate the response over a wide temperature range and the HO and fluxoid models become increasing accurate predictors of the full fluctuation theory. For all values of $\gamma(T = T_c)$, the VOR and HO response well below T_c only match the mean field and fluxoid predictions if T_c is renormalized.

only these terms contribute to the thermodynamic ring-current. If we make an approximation and only include the $l^2/2R_m(0)^2$ terms, where $R_m(0)$ is the value for r that minimizes $V(r)$ when $l = 0$, the current from Eq.

(16) is

$$I_{HO}(T, \phi) = \frac{k_B T}{\Phi_0} \frac{\sum_{l=1}^{\infty} 4\pi l \sin(2\pi l \phi) \exp(l^2 \gamma(T)/2\Lambda(T)^2)}{1 + \sum_{l=1}^{\infty} 2 \cos(2\pi l \phi) \exp(l^2 \gamma(T)/2\Lambda(T)^2)}, \quad (25)$$

which is exactly equivalent the fluxoid current shown in Eq. (11). Through this approximation we are able to show a direct link between the harmonic oscillator approximation to the VOR model and the fluxoid model. Including the second two terms of Eq. (24), which account for the angular momentum dependence of ω and $R_m(l)$, we get

$$Z = \sum_{l=-\infty}^{\infty} \exp(-i2\pi l \phi) \exp(-\gamma(T)^{1/3} V(R_m(l))) \times \frac{\exp(-\gamma(T)^{1/3} \omega/2)}{1 - \exp(-\gamma(T)^{1/3} \omega)}. \quad (26)$$

Using this simplified partition function we can find the ring's current and consequently its susceptibility in the limit where we ignore only quartic fluctuations.

F. Comparison of Models

We have presented the theoretical basis for four models including: the mean field model, the fluxoid model, the harmonic oscillator model and the von Oppen and Riedel model. We now compare the physics captured by each model by plotting the theoretical susceptibility response predicted by each model as a function of temperature for rings with three different $\gamma(T = T_c)$ parameters in Fig. 2.

The mean field model is our baseline. It gives the ring response in the absence of all superconducting fluctuations. At the other extreme, the VOR model incorporates all thermally activated superconducting fluctuations into its derivation of the ring response. In between we have the fluxoid model, which includes only fluxoid fluctuations and the harmonic oscillator model. By comparing these models for rings with different $\gamma(T = T_c)$ we can get a sense of which fluctuations dominate the response.

One striking feature in Fig. 2 in all three plots for all values of $\gamma(T = T_c)$, is that both the VOR model and its HO approximation have an offset in the linear regime, far below T_c , compared to the mean field or fluxoid model. This downshift in T_c appears to reflect a renormalization in T_c due to consideration of all possible fluctuation modes.

Fig. 2(a) shows a ring with $\gamma(T = T_c) = 3$. The low gamma parameter means it has a strong phase stiffness. The susceptibility at $T = T_c$ is 210 nA. We get this number by looking at the value of the VOR model at T_c in Fig.

2(a). We compare this number to $12k_B T/\Phi_0 \approx 120$ nA, for $T = 1.5$ K predicted as the point where we expect a downturn in susceptibility due to fluxoid fluctuations, Eq. (13). Since the fluxoid criterion is smaller than the susceptibility at T_c , susceptibility enhancing amplitude fluctuations at and above T_c overwhelm the susceptibility reduction expected from fluxoid fluctuations. A downturn is not observable, instead the small $\gamma(T = T_c)$ leads to a susceptibility signal above T_c .

When $\gamma(T = T_c) = 3100$, as shown in Fig. 2(b), the fluxoid induced downturn becomes visible below T_c starting at $T \approx 1.52$ K and 120 nA, as predicted by our fluxoid criterion, Eq. (13). All three fluctuation models qualitatively reproduce the shape of the susceptibility suppression. As expected, VOR model predicts a greater susceptibility suppression than the fluxoid or HO models, because only the VOR model includes all thermal fluctuations. The excess suppression between the fluxoid and VOR is presumably due to contributions from non-homogeneous phase winding solutions, amplitude fluctuations, or both. While the excess suppression between the HO and VOR models is due to fluctuations caused by the quartic nature of the potential.

For $\gamma(T = T_c) = 170,000$, shown in Fig. 2(c), the susceptibility response is dominated by fluxoid fluctuations, shown by the almost identical lineshape shared by the fluxoid model and the VOR model. The total response is also well represented by the harmonic oscillator approximation showing that in this region nearly all fluctuations are quadratic in nature.

Fig. 2(c) shows a larger temperature range than the previous panels, and the GL approximation that T is close to T_c is not valid over the whole plot. GL theory is strictly valid in the range of temperature where the linear mean field response approximates a temperature dependence that goes as $(1 - t^4)$, $t = T/T_c$, shown as an orange dotted line. An alternative criterion is that $T > \Delta(T)$, where $\Delta(T)$ is the superconducting gap. These both result in approximately the same range of validity. GL theory has been applied with success at temperatures far from T_c , but interpretation of results in this regime should be treated with caution. The $(1 - t^4)$ dependence is not included in panels (a) and (b) because all plotted temperatures lie within the valid range.

In the next section we describe our measurement of ring susceptibility for rings with different $\gamma(T = T_c)$ values. We find good agreement between our data and the fluctuation response predicted by the fluxoid and VOR models.

III. SAMPLE AND MEASUREMENT TECHNIQUE

A. Sample Preparation

We measured quasi-one-dimensional superconducting rings in a dilution refrigerator⁴⁰ with a scanning SQUID

susceptometer⁴¹ that was explicitly designed for this purpose. We focus on data from two different samples expected to exhibit fluxoid fluctuations. Sample I's rings were fabricated and measured previously.³³ The rings were narrow and dirty with $T_{cI} \approx 1.5$ K. They were made by depositing a 40 nm thick Aluminum film by e-beam evaporation at a rate of about 1 Å/s and a pressure of approximately 10^{-6} mBar on a Si substrate patterned with poly(methyl methacrylate) (PMMA) resist. During the deposition, the rate temporarily dropped to a negligible level for about 10 min and subsequently recovered. This delay caused the formation of two superconducting layers separated by an AlOx tunneling barrier. The coupling between the two Al layers depended on the width of the rings with narrow rings ($w \leq 190$ nm) and wide rings ($w \geq 250$ nm) showing a single order parameter. Intermediate widths showed evidence of weak interactions between the two layers leading to two order parameter effects.³³ In this work we only present data from the narrow rings which showed no two order parameter behavior. However, due to the oxidation process we suspect the thinnest rings have a large oxidized layer that reduces the thickness of the superconductor. Consequently we expect that these rings have an effective height that is less than 40 nm. We can test this prediction by extracting the ring's cross-section from fits to the VOR model.

The rings on sample II were fabricated specifically for this paper. The fabrication process was almost identical to the rings from sample I except the evaporated film was thinner, $d = 15$ nm, and there was no interruption in the evaporation. The deposited rings were wide and dirty with $T_{cII} \approx 2.1$ K. Of the many fabricated rings of different widths and radii, only the widest rings, $w \approx 850$ nm, had a diamagnetic response. The next widest rings, $w \approx 450$ nm, showed no signs of superconductivity indicating that they were oxidized throughout. This evidence makes it difficult to predict with certainty what portion, if any, of the 850 nm rings are also oxidized. Although the 1D approximation, $w \gg \xi(T)$, is no longer strictly valid for these rings the theory still provides a good fit to our data. For each sample we used Ginzburg Landau models^{20,33,37} to fit a zero temperature penetration depth $\lambda_I(0) \approx 800$ nm, $\lambda_{II}(0) \approx 1.5$ μ m, and coherence length $\xi_I(0) \approx 80$ nm, $\xi_{II}(0) \approx 30$ nm.

B. Measurement

Our measurements are done with a voltage biased DC SQUID susceptometer amplified by a series-array SQUID preamplifier.⁴² The SQUID is mounted on a piezo-resistive scanning assembly⁴⁰ which is connected to the mixing chamber of a dilution refrigerator through a single copper braid. The temperature of the scanner and sample is controlled with sub-milikelvin precision through feedback. The SQUID sensor's counter-wound geometry, with on-sensor modulation coils for feedback, enable cancellation of an applied field to one part in 10^4 .⁴¹ The

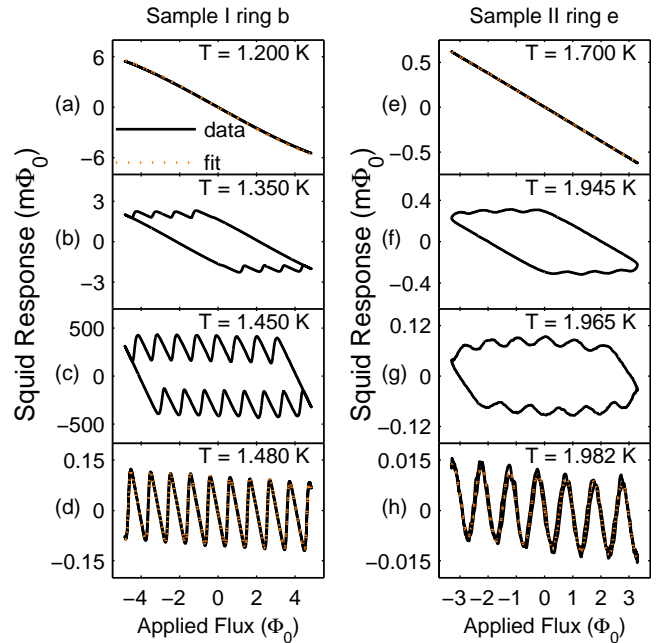


FIG. 3: (Color Online) Plots of SQUID response vs. applied flux at different temperatures for a ring from each of the two samples. Rings b and e refer to specific rings plotted in Fig. 4. Ring b $T_c = 1.56$ K and ring e $T_c = 2.08$ K. The curves evolve from non-hysteretic with no fluxoids at low temperatures, through a hysteretic regime, to non-hysteretic with a change in fluxoid number at every applied flux quantum near T_c . The orange dotted lines are fits to the GL current, Eq. (10) at low temperatures and to the Boltzmann distribution, Eq. (11), at high temperatures. We extract the ring's susceptibility at each temperature by taking the derivative at $\phi = 0$.

ring current is measured by positioning the SQUID about 1 μ m above the ring and recording the flux induced by the ring's current in the SQUID's 4.6 μ m diameter pick-up loop. During the measurement, the applied flux threading the ring is varied by several flux quanta at a few Hertz by an on-sensor field coil. This measurement is repeated 13 μ m above the ring and the ring signal is computed as the difference between the two positions for each value of applied flux. This procedure allows us to achieve an additional three orders of magnitude of background cancellation. A more detailed description of the measurement system was given by Koshnick *et al.*³²

We plot the flux induced in the SQUID's pick-up loop as a function of the flux applied by the field coil in Fig. 3 for two different rings. The measurement is repeated to record the full temperature dependence of the ring's response. The ring current, I , is coupled as flux into the SQUID pick-up loop through the mutual inductance, M . $\Phi_{\text{SQUID}} = MI$. We estimate the mutual inductance between the SQUID pick-up loop and a ring by calculating the mutual inductance between two on axis rings with

radii r_1 and r_2 a distance z apart.

$$M = \pi\mu_0 r_1 r_2 \int_0^\infty d\kappa e^{-\kappa|z|} J_1(\kappa r_1) J_1(\kappa r_2) \quad (27)$$

J_1 is a Bessel function of the first kind. For all our mutual inductance calculations we assume a ring-pick-up loop separation of $1\mu\text{m}$. Through a separate fitting technique³³ we estimate the actual distance between the pick-up loop and the ring to range from $0.75 - 1.1\mu\text{m}$. Ring currents and susceptibilities quoted later in this paper have error bars that reflect this systematic uncertainty in the coupling factor which would shift the entire dataset. For example, the ring-SQUID mutual inductance between a ring with a radius of $1.5\mu\text{m}$ positioned $1\mu\text{m}$ above the SQUID's pick-up loop is $M = 0.718\Phi_0/\text{nA}$. The error on the height from $0.75 - 1.1\mu\text{m}$ gives $M = 0.669 - 0.849\Phi_0/\text{nA}$, but because the SQUID is kept a constant distance from the ring for all data points taken at the same time on the same ring this systematic error in the height would shift all data points together.

The ring response curves plotted in Fig. 3 evolve from cubic and non-hysteretic at low temperatures through a hysteretic regime to periodic and non-hysteretic near T_c . At low temperatures the current response is well described by the GL current with no phase windings, Eq. (10) with $n = 0$, shown as a orange dotted line in panels (a) and (e) of Fig. 3. As the temperature increases the applied flux causes the ring to transition to higher fluxoid states; however, the phase slip rate becomes comparable to the measurement time only at large applied flux, thus leading to a hysteretic response.

Finally, as the temperature approaches T_c the phase slip rate becomes fast compared to the measurement time at small applied flux and the ring relaxes to thermal equilibrium. Thermal fluctuations are strong enough for transitions to occur within some range of $\phi = m/2$ where m is an odd integer. The ring's response is no longer hysteretic and can be approximately modeled as a Boltzmann distribution of all fluxoid states, Eq. (11), shown as a orange dotted line in panels (d) and (h) of Fig. 3. We extract the magnetic susceptibility of the ring at each temperature by fitting a low order polynomial to obtain the slope at $\phi = 0$.

C. Susceptibility Data

We measured thirty-eight rings on sample I and twelve rings on sample II. Sample I was fabricated and measured primarily for a different experiment.³³ As a result only eight of the rings measured have sufficient susceptibility data over a wide enough temperature range to test the theories presented in the previous section. Two representative rings were selected for this paper. The three rings from Sample II were chosen to show a variety of ring parameters, and because they had the most dense susceptibility data over the important temperature

range. The set of five rings allows us to explore the effects of ring size and cleanliness on the fluctuation response. Fig. 4 shows the susceptibility vs. temperature data for those five rings. Each of the ring's physical parameters are given in table I. We extracted the ring radii from the flux periodicity of the ring's response in thermal equilibrium and confirmed the measurement through SEM imaging. The ring thicknesses were measured with an AFM, and the width with SEM. Fitting to the VOR model allowed us to estimate values for the ring's cross-section and mean free path. We used the measured ring width and thickness plus an additional error factor as an upper limit on the cross-section parameter in the VOR model for rings (c-e). No lower limit was enforced due to the possibility of oxidation reducing the superconducting cross-section.

Ring	Directly Measured			Extracted from VOR fits			
	R (μm)	w (nm)	d (nm)	wd (nm^2)	95% CI	ℓ_e (nm)	95% CI
a(I)	0.496	123	40	1598	1140-2314	6.4	4.3-9.4
b(I)	1.97	90	40	583	492-1177	8.5	4.4-10.4
c(II)	1.21	840	15	13319	2811 -14790	0.11	0.09-0.48
d(II)	1.75	850	15	14790	11896-14790	0.08	0.07-0.11
e(II)	1.82	850	15	13602	9172 -14790	0.08	0.07-0.12

TABLE I: Table of ring values. Values for the cross-section and mean free path, extracted from fits to the VOR model, are given with their 95% confidence interval. An upper limit of 14790 nm^2 was enforced on the ring cross-section to constrain the fits for rings (c-e).

Ring	$T_c(\text{K})$	95% CI
a(I)	1.556	1.554-1.557
b(I)	1.555	1.550-1.556
c(II)	2.076	2.072-2.086
d(II)	2.074	2.066-2.083
e(II)	2.080	2.075-2.086

Ring	$\gamma(T = T_c)$	95% CI	$E_0(T = 0)$	95% CI
a(I)	9.20	6-14	2138	1850-2550
b(I)	899	760-1660	898	820-1300
c(II)	78×10^3	$(18 - 95) \times 10^3$	2650	1180-2870
d(II)	353×10^3	$(261 - 443) \times 10^3$	2590	2280-2730
e(II)	438×10^3	$(294 - 536) \times 10^3$	2370	1910-2550

TABLE II: Table of fitted values. We used the temperature independent portions of $\gamma(T)$ and $E_0(T)$ as fit parameters in the VOR model. This table reports values for $\gamma(T = T_c)$ and $E_0(T = 0)$ as well as the limits of the 95% confidence interval obtained from bootstrap analysis for the data presented in Fig. 4.

Fig. 4 plots the susceptibility vs. temperature curves for five rings. The blue susceptibility data points represent the slope at $\phi = 0$ of the SQUID response at different

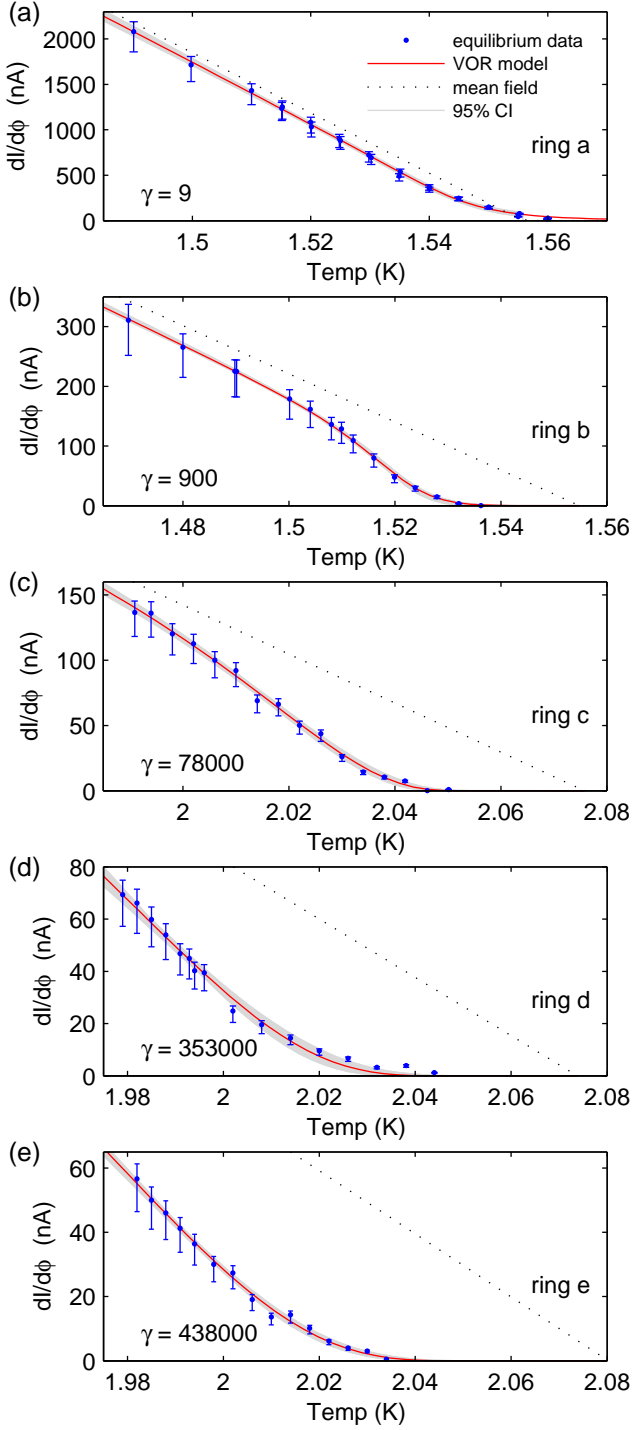


FIG. 4: (Color Online) Zero field susceptibility (blue dots) vs. temperature plotted for five different rings. In all plots the solid red line is a fit to the VOR model, Eqs. (20, 21). The dotted black line is the expected mean field susceptibility given by $I^0(T)$, Eq. (9). The gray shaded area represents the 95% confidence interval from bootstrapping. The error bars represent the systematic uncertainty in the SQUID-ring mutual inductance.

temperatures scaled by the ring-SQUID mutual inductance to get the ring current. The error bars represent height errors in our calculation of the mutual inductance, Eq. (27). This error is systematic and expected to be the same for all points in a panel. Using T_c , and the temperature independent portions of $\gamma(T)$ and $E_0(T)$ as the free parameters, the red line is a fit of the data to the VOR model, Eqs. (20, 21). The fit results used to generate the red curves are given in table II. We report values for $\gamma(T)$ at T_c and $E_0(T)$ at $T = 0$. The reported T_c represents the nominal mean field T_c entering the VOR model.² The fitted values of $\gamma(T = T_c)$ are also listed on each of the plots. The black dotted line is the mean field ring response, Eq. (9), which one would expect if no fluctuations were present. Deviations in the data from the black dashed line show the influence of fluctuations on a given ring. Finally, the gray region of the curve is the 95% confidence interval (CI) obtained from bootstrapping.

Using the fit results from table II along with the known values of the ring radii given in table I we can extract values for the ring's cross-section and mean free path from expressions for $E_0(T)$, Eq. (15), and $\gamma(T)$, Eq. (22). The ring parameters obtained in this way are given along with their 95% confidence intervals in table I. Due to the evaporation conditions discussed previously, we're not confident that the entire cross-section of each ring is superconducting. For the two rings on sample I the fitted cross-sections are smaller than the values found using AFM/SEM, which confirms our suspicion that a portion of the ring is oxidized. The data from the three sample II rings is within the downturn region, i.e. the decrease in the susceptibility is not linear even at the lowest plotted temperatures. Practically we are limited on the low end of the temperature range by the point where the SQUID response curves go hysteretic. A three parameter fit is under-constrained and it is consequently difficult to get accurate VOR fits without susceptibility data at lower temperatures including the point where the data is reduced from the linear response.

As a result, for rings (c-e) we put a strict upper limit of $w \times d = 14790$ nm on the cross-section, which acted as an additional constraint on the VOR fits. The cross-sections extracted from fits to the constrained VOR model for the rings on sample II agree well with the AFM/SEM cross-section indicating little oxidation. A similar limit was not applied to rings (a-b) because data in the linear susceptibility region kept the fit from being under-constrained.

The agreement between the susceptibility data and fits to the VOR model are good for all rings except ring (d), where it is clear that the VOR model does not capture the shape of the data at high temperatures. It is unclear why the VOR model provides a poor fit for this ring. It is possible that errors from extracting the susceptibility near T_c , errors that are not accounted for in the error bars, are particularly large for measurements on this ring.

Looking at the sequence of five rings it is clear that the extent of the suppression of superconductivity increases as $\gamma(T = T_c)$ increases. This is just what we expect for

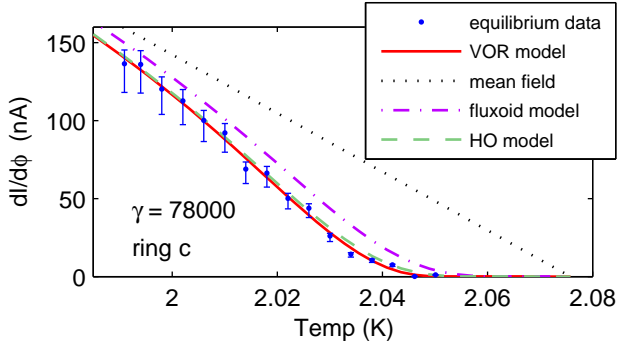


FIG. 5: (Color Online) Comparison of the four models plotted using parameters obtained from fitting the data from ring (c) to the VOR model. Fitting to the fluxoid model would yield an equally good fit with a slightly different T_c .

a series of rings where fluxoid fluctuations play a larger and larger role.

Ring (a) shows an enhancement of the superconducting response above T_c . This response is caused by amplitude fluctuations and has been studied by Koshnick *et al.*³² and Zhang and Price.²⁰ As we showed in our description of the theoretical models only the VOR model can correctly reproduce the upturn in susceptibility above T_c . The fluxoid fluctuation model cannot reproduce a current above T_c and will fail for any ring with a $\gamma(T_c) < 40$.

The remaining four rings in Fig. 4 show a suppression of the susceptibility signal below the mean field response (shown in black dots). However, of the plotted rings only ring (b) has a large enough temperature range to observe a downturn from the linear regime. The full temperature range plotted for rings (c-e) is already deep in the suppression region. This is due to the fact that $\gamma(T_c) > 16,000$ for rings (c-e). In the next section we expand the temperature range by adding susceptibility data from lower temperature hysteretic ring response curves, to confirm that the response is suppressed from the mean field value. The downturn for ring (b) occurs at $T \approx 1.52$ K and 120 nA, which corresponds to the criterion for fluxoid fluctuations given in Eq. (13). Such agreement validates our criterion for the onset of susceptibility suppression driven by fluxoid fluctuations.

We have shown that the VOR model describes the temperature dependence of the susceptibility. To get a feeling for the type of fluctuations that play a role in the ring response we plot the fluxoid model and the HO model in addition to the VOR model and mean field model for ring (c) in Fig. 5. It is clear that fluxoid fluctuations cause the majority of the suppression, with quadratic fluctuations described by the HO model contributing to the renormalization of T_c and quartic fluctuations described by the VOR model playing only a minor role. In fact the fluxoid model would fit the data equally well with just a shift in the T_c .

The dataset, taken as a whole, confirms the points

we made throughout this paper. Fluxoid fluctuations not only suppress the rings superconducting response but play an increasingly large role in the suppression as $\gamma(T = T_c)$ increases. We showed that our susceptibility vs. temperature data is well described by a GL model for homogeneous rings, developed by von Oppen and Riedel,² that includes all thermally activated fluctuations, but the largest gamma rings can be equally well described by our simple fluxoid only model with a shifted T_c . Furthermore we can use fits to the VOR model to reproduce some of the rings physical parameters including the cross-section and mean free path. Finally, by using VOR fit parameters we can employ our two approximate models, the fluxoid model, and the harmonic oscillator model, to determine how much of the suppression is due to either fluxoid fluctuations or quartic fluctuations, done for ring (c) in Fig. 5.

D. Hysteretic Susceptibility Data

For rings (c-e) in Fig. 4 we expect the onset of the downturn induced by fluxoid fluctuations in a temperature range where the SQUID response curves are hysteretic, as shown in Fig. 3. This is due to the fact that in these thinnest, dirtiest rings $L \gg \xi(T)$ and fluxoid fluctuations are already energetically favorable at the temperature when phase slips begin to occur, as discussed in Sec. II B. Fluxoid fluctuations are never energetically favorable for ring (a) and they onset well after phase slips in ring (b). Phase slips onset at ~ 1.3 K while fluxoid fluctuations onset at ~ 1.51 K.

To demonstrate that the data presented represents a real reduction in the ring response we examine the susceptibility signals at lower temperatures that fall in the hysteretic regime. We evaluate susceptibility in the hysteretic regime by taking the slope at zero current on the long continuous sides of the hysteretic curves. These susceptibility data points are shown as green dots in Fig. 6.

Fig. 6 shows susceptibility data in the hysteretic regime (green points) and reproduces the susceptibility data from the non-hysteretic regime (blue points) from rings (b-e) in Fig. 4. Fig. 6 also shows the $(1 - t^4)$ dependence, plotted as an orange dotted line, that sets the validity of our GL based models. In Panel (a) the susceptibility in the hysteretic regime has dropped below the mean field prediction and instead closely follows the $(1 - t^4)$ curve.

Notice that the hysteretic data points in rings (c-e), panels (b-d), follow the mean field curve until a crossover point when they line up with the VOR model and the higher temperature susceptibility data. This provides evidence that the susceptibility measured from the SQUID response curves in thermal equilibrium is suppressed from the mean field value. The drop in susceptibility from the mean field value occurs when phase slips occur at a sufficiently high rate and multiple fluxoid states compete to suppress the response.

IV. CONCLUSIONS

Superconducting phase slips in one dimensional rings and wires have been the subject of theoretical and experimental interest for decades. While phase slips in 1D structures determine the onset of resistance, the fluxoid processes we described here cause the loss of another hallmark of superconductivity, the ability to screen magnetic field. In this paper we have outlined four models that describe the effects of superconducting fluctuations on the susceptibility response in rings. We have shown that ring responses for rings with various physical parameters can be characterized by a model by von Oppen and Riedel for uniform rings that includes all thermal fluctuations. However, by comparing the models we can determine the types of fluctuations that contribute to the response of a given ring. We specifically found that for rings with weak phase stiffness the ring response can be described using a fluxoid only model, indicating that these types

of fluctuations are the dominant cause of suppression of the susceptibility signal. One could imagine extending this ring system to a weakly connected grid, linking our results to the field of percolation superconductivity. Additionally, achievable experimental conditions allow fluxoid fluctuations to occur at temperatures down to 50 mK, which could provide an experiment setup for examining the quantum mechanical behavior of a 1D ring.⁴³

Acknowledgments

This work was supported by NSF Grants DMR-0803974, DMR-0507931, PHY-0425897 and by the Packard Foundation. Work was performed in part at the Stanford Nanofabrication Facility, which is supported by NSF Grant No. ECS-9731293, its lab members, and industrial affiliates. We express gratitude to Martin Huber for assistance in SQUID design and fabrication.

-
- * Now at: Department of Physics, Harvard University
 † Electronic address: kmoler@stanford.edu
- ¹ N. C. Koshnick, *Nano-SQUID Susceptometry and Fluctuation Effects in Superconducting Rings*, Ph.D. thesis, Stanford University (2009).
 - ² F. von Oppen and E. K. Riedel, Phys. Rev. B, **46**, 3203 (1992).
 - ³ W. Skocpol and M. Tinkham, Rep. Prog. Phys., **38**, 1049 (1975).
 - ⁴ V. Emery and S. Kivelson, Nature, **374**, 434 (1995).
 - ⁵ J. M. Kosterlitz and D. J. Thouless, J. Phys. C: Solid State Phys., **6**, 1181 (1973).
 - ⁶ T. M. Rice, Phys. Rev., **140**, A1889 (1965).
 - ⁷ J. S. Langer and V. Ambegaokar, Phys. Rev., **164**, 498 (1967).
 - ⁸ D. E. McCumber and B. I. Halperin, Phys. Rev. B, **1**, 1054 (1970).
 - ⁹ N. Giordano, Phys. Rev. Lett., **61**, 2137 (1988).
 - ¹⁰ C. N. Lau, N. Markovic, M. Bockrath, A. Bezryadin, and M. Tinkham, Phys. Rev. Lett., **87**, 217003 (2001).
 - ¹¹ B. J. Baelus, F. M. Peeters, and V. A. Schweigert, Phys. Rev. B, **61**, 9734 (2000).
 - ¹² J. Berger, Phys. Rev. B, **67**, 014531 (2003).
 - ¹³ H. Bluhm, N. C. Koshnick, M. E. Huber, and K. A. Moler, arXiv.org:0709.1175 (2007).
 - ¹⁴ S. Pedersen, G. R. Kofod, J. C. Hollingbery, C. B. Sørensen, and P. E. Lindelof, Phys. Rev. B, **64**, 104522 (2001).
 - ¹⁵ D. Y. Vodolazov, F. M. Peeters, S. V. Dubonos, and A. K. Geim, Phys. Rev. B, **67**, 054506 (2003).
 - ¹⁶ J. E. Lukens and J. M. Goodkind, Phys. Rev. Lett., **20**, 1363 (1968).
 - ¹⁷ A. D. Hernández, B. J. Baelus, D. Domínguez, and F. M. Peeters, Phys. Rev. B, **71**, 214524 (2005).
 - ¹⁸ M. Morelle, D. S. Golubović, and V. V. Moshchalkov, Phys. Rev. B, **70**, 144528 (2004).
 - ¹⁹ V. Bruyndoncx, L. Van Look, M. Verschuere, and V. V. Moshchalkov, Phys. Rev. B, **60**, 10468 (1999).
 - ²⁰ X. Zhang and J. C. Price, Phys. Rev. B, **55**, 3128 (1997).
 - ²¹ J. R. Kirtley, C. C. Tsuei, V. G. Kogan, J. R. Clem, H. Raffy, and Z. Z. Li, Phys. Rev. B, **68**, 214505 (2003).
 - ²² J. Berger and J. Rubinstein, Phys. Rev. B, **56**, 5124 (1997).
 - ²³ L. D. Jackel, W. W. Webb, J. E. Lukens, and S. S. Pei, Phys. Rev. B, **9**, 115 (1974).
 - ²⁴ A. Kanda, B. J. Baelus, D. Y. Vodolazov, J. Berger, R. Furgun, Y. Ootuka, and F. M. Peeters, Phys. Rev. B, **76**, 094519 (2007).
 - ²⁵ D. Y. Vodolazov, F. M. Peeters, T. T. Hongisto, and K. Y. Arutyunov, Europhys. Lett., **75**, 315 (2006).
 - ²⁶ D. Y. Vodolazov, B. J. Baelus, and F. M. Peeters, Phys. Rev. B, **66**, 054531 (2002).
 - ²⁷ R. S. Newbower, M. R. Beasley, and M. Tinkham, Phys. Rev. B, **5**, 864 (1972).
 - ²⁸ K. Arutyunov, D. Golubev, and A. Zaikin, Phys. Rep., **464**, 1 (2008).
 - ²⁹ V. Ambegaokar and U. Eckern, Phys. Rev. B, **44**, 10358 (1991).
 - ³⁰ V. Ambegaokar and U. Eckern, Europhys. Lett., **13**, 733 (1990).
 - ³¹ G. Schwiete and Y. Oreg, Phys. Rev. Lett., **103**, 037001 (2009).
 - ³² N. C. Koshnick, H. Bluhm, M. E. Huber, and K. A. Moler, Science, **318**, 1440 (2007).
 - ³³ H. Bluhm, N. C. Koshnick, M. E. Huber, and K. A. Moler, Phys. Rev. Lett., **97**, 237002 (2006).
 - ³⁴ X. Zhang, *SQUID Microsusceptometry of Mesoscopic Superconducting Rings*, Ph.D. thesis, University of Colorado (1996).
 - ³⁵ W. A. Little, Phys. Rev., **156**, 396 (1967).
 - ³⁶ N. Byers and C. N. Yang, Phys. Rev. Lett., **7**, 46 (1961).
 - ³⁷ M. Tinkham, *Intorduction to Superconductivity 2nd edition* (Dover Publications, 2004).
 - ³⁸ D. J. Scalapino, M. Sears, and R. A. Ferrell, Phys. Rev. B, **6**, 3409 (1972).
 - ³⁹ S. Bell, J. Phys. B: Atom. Molec. Phys., **3**, 745 (1979).
 - ⁴⁰ P. G. Bjornsson, B. W. Gardner, J. R. Kirtley, and K. A.

- Moler, Rev. Sci. Inst., **72**, 4153 (2001).
- ⁴¹ M. E. Huber, N. C. Koshnick, H. Bluhm, L. J. Archuleta, T. Azua, P. G. Björnsson, B. W. Gardner, S. T. Halloran, E. A. Lucero, and K. A. Moler, Rev. Sci. Inst., **79**, 053704 (2008).
- ⁴² M. E. Huber, P. A. Neil, R. G. Benson, D. A. Burns, A. F. Corey, C. S. Flynn, Y. Kitaygorodskaya, O. Massihzadeh, J. M. Martinis, and G. C. Hilton, Applied Superconductivity, IEEE Transactions on, **11**, 4048 (2001).
- ⁴³ K. A. Matveev, A. I. Larkin, and L. I. Glazman, Phys. Rev. Lett., **89**, 096802 (2002).

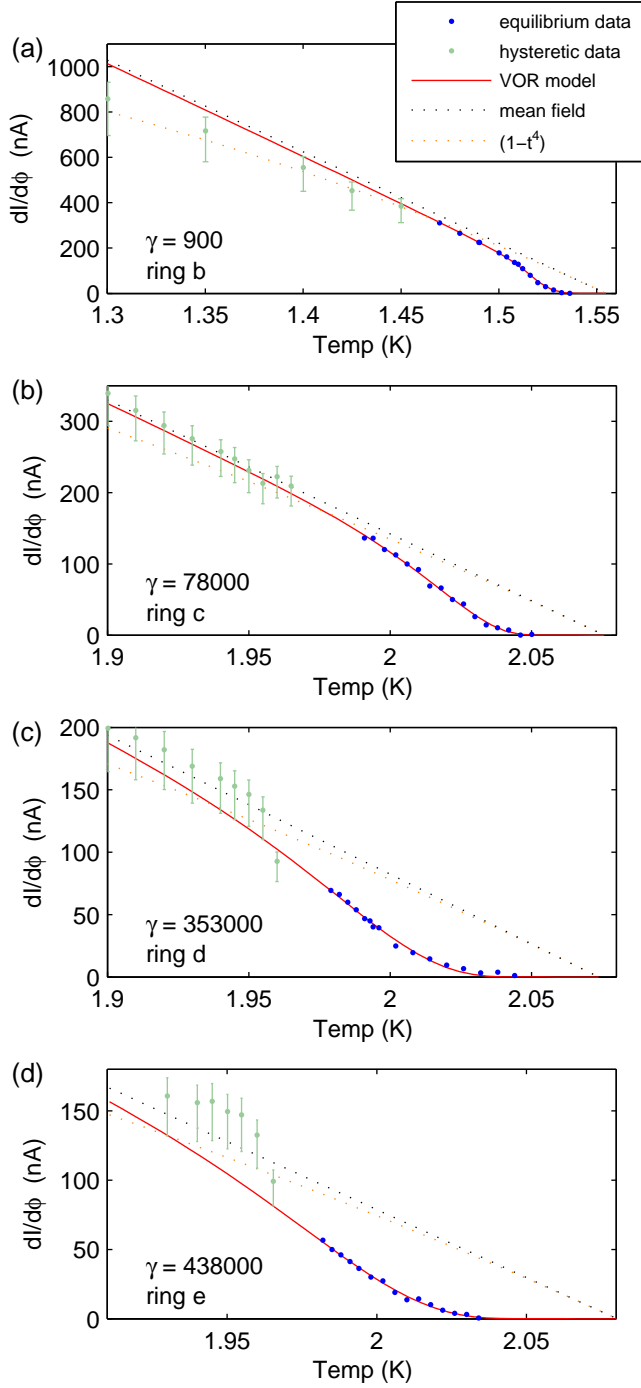


FIG. 6: (Color Online) Susceptibility data from rings (b), (c), (d) and (e). The green points represent the slopes of the hysteretic curves, which estimate the susceptibility in the hysteretic regime. The error bars account for a systematic error in the coupling constant that would shift all points together. The blue points give the susceptibility of the ring's response in thermal equilibrium. The red solid line is a fit of the blue non-hysteretic data to the VOR model and the black dotted line is the mean field response. Also plotted is the $(1 - t^4)$ temperature dependence which places approximate limits on the validity of GL.